International Core Journal of Engineering Volume 10 Issue 7, 2024
ISSN: 2414-1895 DOI: 10.6919/ICJE.202407_10(7).0010

Study on Section Classification of High-Strength Steel and Ultra-High-Strength Steel Bent Members

Yuying Guo

Key Laboratory of Urban Security and Disaster Engineering of Ministry of Education, Beijing University of Technology, Beijing 100124, China

Abstract

To provide recommendations on the cross-sectional classification and width-thickness ratio limits for bent members made of high-strength steel and ultra-high-strength steel, a numerical simulation approach was employed. Using ABAQUS finite element software, finite element models of I-shaped bent members made of high-strength steel and ultra-high-strength steel were established based on four-point bending test specimens. The accuracy of the models was verified by comparing them with experimental results, taking into account factors such as welding residual stress, local initial geometric defects, steel strength, and plate width-thickness ratio. Following the principle of equivalent strength and considering the interaction between flanges and webs, recommendations on the cross-sectional classification and width-thickness ratio limits for bent members made of high-strength steel and ultra-high-strength steel were proposed and subjected to applicability evaluation. The results indicate that the proposed cross-sectional classification and width-thickness ratio limits, which consider plate interactions, can accurately predict the load-carrying capacity and plastic deformation rotation capacity of bent members made of high-strength steel and ultra-high-strength steel.

Keywords

High-Strength Steel; Ultra-High-Strength Steel; Bent Members; Parameter Analysis; Section Classification; Width-Thickness Ratio Limit.

1. Introduction

As technological advancements progress, the strength of steel materials has been steadily increasing. Steel is classified as high-strength steel when its yield strength (f_y) reaches or exceeds 460 MPa[1], and as ultra-high-strength steel when the yield strength exceeds 690 MPa. Known for its superior strength, excellent weldability, and the ability to reduce construction volume, high-strength steel has increasingly gained attention and is being widely adopted in various applications.

In the application of steel structures, design methods based on section classification have become a principal approach in steel structure design[2]. In China, the 'Steel Structure Design Standard' GB 50017-2017[3] (hereinafter referred to as the 'new steel standard') introduces a systematic design method based on section classification for seismic performance, dividing sections into five categories based on the impact of local buckling on section performance. Each section category corresponds to a different design method, covering up to the Q460 steel grade. The 'Design Standard for High-Strength Steel Structures' JGJT 483-2020[4] stipulates that the section classification for high-strength steel components should be designed entirely in accordance with the 'new steel standard'. However, high-strength steel exhibits characteristics such as a higher yield-to-tensile strength ratio, marked nonlinearity, less pronounced strain-hardening effects, and reduced ductility, which means its section load-bearing capacity and plastic deformation rotation capacity differ from those of ordinary steel sections.

ISSN: 2414-1895 DOI: 10.6919/ICJE.202407_10(7).0010

I-shaped sections, known for their excellent performance and cost-effectiveness, are commonly utilized in engineering. Bending members are critical energy-dissipating components in steel structures, prompting both domestic and international scholars to explore section classification of I-shaped bending members extensively. McDermott[5-6] performed three-point and four-point bending tests on 690 MPa high-strength steel beams, establishing the limits for the width-to-thickness ratio of flanges in I-shaped sections to prevent plastic buckling. D.Beg[7] conducted both four-point bending tests and numerical simulations on 700 MPa high-strength steel I-shaped beams, discovering that the interaction between the flanges and the web enhances the beams' plastic rotational capacity. Ricles[8] and Earls[9] performed three-point bending tests on 550 MPa I-shaped beams, indicating that the yield-to-tensile strength ratio, lateral supports, section dimensions, and initial imperfections impact the rotational capacity. They suggested that the American standard AISC-LRFD should revise the height-to-thickness ratio limits for high-strength steel webs. Thomas[10] and Shokouhian[11] revised the section limits for I-shaped beams of 483 MPa and 345 MPa, 460 MPa grades, respectively. Tong and Fu[12] performed nonlinear analyses on uniformly compressed and bent rectangular plates with different boundary conditions at 235 MPa, proposing a section classification method tailored for seismic design of steel components. Peng[13] conducted numerical simulations on 690 MPa I-shaped beams, noting that while they demonstrate ductility, achieving a rotational capacity (R) exceeding 3 is challenging. Xu[14] and Han[15] analyzed I-shaped beams of 460 MPa, 550 MPa, 690 MPa, 800 MPa, and 960 MPa high-strength and ultra-high-strength steel, recommending that the interaction between flanges and webs be considered and proposing a formula that integrates the normalized width-to-thickness ratios of flanges and webs for classification limits.

The existing research primarily focuses on ordinary steel, 460 MPa grade steel, and 690 MPa grade steel, with less attention given to steels exceeding 690 MPa. Moreover, the current methodologies for section classification are insufficient. When bending members are loaded, and flanges undergo local buckling, the web also deforms to coordinate with the flange. This deformation of the web is passively induced to accommodate the flange's deformation, indicating a constraining effect on the flange's deformation, and vice versa; there is an interrelation between them[16]. Previous studies[6-16] have shown that the interaction between flanges and webs should not be overlooked. However, current research and some international standards employ a singular plate rule for section classification, treating the web as a simply supported single plate on all four sides and the flange as a three-side supported, one-side free single plate, thereby neglecting the interrelation between the flange and the web. This approach fails to consider how differences in width-to-thickness ratios between the flange and web alter their mutual support, leading to a change in their actual boundary conditions[2]. Some standards that account for the mutual influence of flanges and webs feature section classification formulas for width-to-thickness limits that are complex and not user-friendly for practical engineering applications.

Overall, the current section classification for high-strength steel bending members is limited, and there is a lack of section classification for ultra-high-strength steel bending members. Therefore, there is an urgent need to conduct research on the section classification of high-strength and ultra-high-strength steel bending members.

This paper investigates the section classification of high-strength and ultra-high-strength steel I-shaped bending members, covering steel grades Q460, Q550, Q690, Q800, Q960, and Q1100. It examines the effects of welding residual stress, local initial geometric imperfections, steel grades, and plate width-to-thickness ratios on the load-bearing capacity and rotational ability of high-strength and ultra-high-strength steel I-shaped bending members. Based on extensive parametric analysis results and referencing the section classification philosophy of the 'Steel Structure Design Standard' GB50017-2017[3], this study considers the interaction between the flanges and webs. It proposes section classifications and width-to-thickness ratio limitations for high-strength and ultra-high-strength steel bending members, providing references for the seismic performance-oriented design and application of high-strength and ultra-high-strength steel components.

ISSN: 2414-1895 DOI: 10.6919/ICJE.202407_10(7).0010

2. Numerical Simulation Study

To propose the cross-section classification recommendations for I-shaped cross-section bending members made of high-strength and ultra-high-strength steels and investigate the impact mechanisms of related factors on the sectional performance of these steels, it is necessary to calculate the sectional bearing capacity and plastic deformation rotational capacity of the members. Therefore, numerical simulation methods are used, employing the S4R shell element in ABAQUS finite element software for finite element modeling of I-shaped cross-section bending members. This approach yields a validated and effective finite element model, enabling extensive parametric analysis to provide data support for subsequent cross-section classification.

2.1 Finite Element Model

This finite element model replicates the four-point bending tests conducted on I-shaped cross-section bending members fabricated from high-strength and ultra-high-strength steels. The experimental setup follows the protocol of the four-point bending tests detailed in Reference [15], as depicted in Fig. 1. The boundary conditions for the test specimen are simply supported, utilizing curved bearings. Lateral stability is ensured by side reaction columns that prevent out-of-plane torsion at the ends of the members. Vertical loads are uniformly applied at the third points of the member using a load distribution beam. As prescribed in Reference [15], the four-point bending test design and corresponding computational model are illustrated in Fig. 2, with the finite element model shown in Fig. 3. The model's boundary conditions mirror those of the experiments detailed in Reference [15], featuring coupling at the mid-span loading point on the loading plane to avoid stress concentration. Identical concentrated forces, denoted as P, are applied at coupling points RP1 and RP2. The supports are designed to be simply supported, which is achieved by constraining translational movements in the X, Y, and Z directions and rotational movements in the Y and Z directions at the bottom nodes of the stiffener ribs on the left support end. The simulation of the right support end is achieved by limiting translational movements in the X and Y directions and rotational movements in the Y and Z directions at the bottom nodes of the stiffener ribs. Besides the main supports, lateral bracing is positioned at both sides of the loading points to restrict the translational movement in the X direction at the bracing points. Furthermore, the translational movement in the X direction is restricted at the junction between the flange and the web in the pure bending section at mid-span to prevent lateral instability.

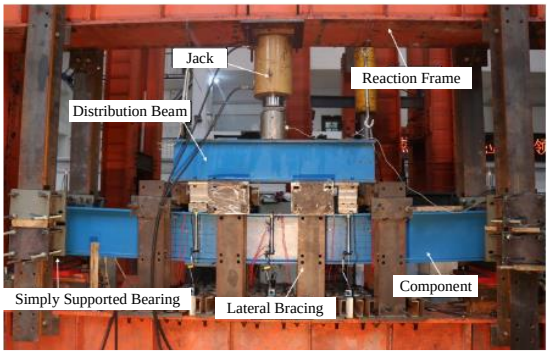

Fig.1 Four-point bending test loading apparatus

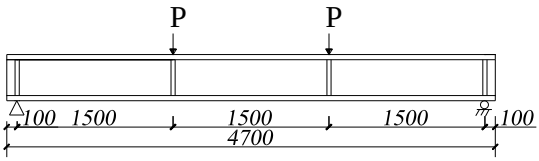

Fig.2 Computational model

ISSN: 2414-1895 DOI: 10.6919/ICJE.202407_10(7).0010

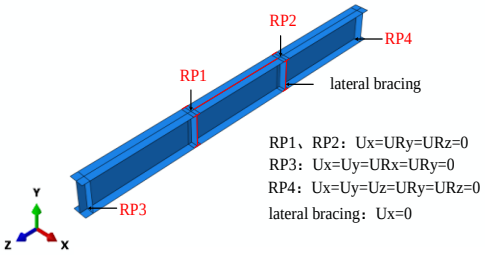

Fig.3 Finite element model schematic

The accuracy of the material constitutive model is crucial for the sectional bearing capacity and post-yield plastic deformation ability of bending members. This paper focuses on steel components of grades Q460, Q550, Q690, Q800, Q960, and Q1100. According to the "Design Standard for High Strength Steel Structures" JGJT 483-2020 [4], a four-linear model with a yield plateau is used for Q460 steel, while a three-linear model without a yield plateau is adopted for steels above Q460. For consistency and applicability in subsequent calculations, parameters from Reference[4] are used for Q460 to Q690 steels, while material properties for Q800 and Q960 steels are determined according to Reference[17], and those for Q1100 are based on experimental results from Reference[18], as shown in Table 1.

Table 1. Material parameters of steel

	Q460	Q550	Q690	Q800	Q960	Q1100
Elastic Modulus (E/MPa)	206000					
Yield Strength (f_y/MPa)	460	550	690	800	960	1100
Strain at End of Yield Plateau (ε_{st})	0.02	-	-	-	-	-
Ultimate Strength (f_u/MPa)	550	670	770	840	980	1418
Ultimate Strain (ε_u)	0.12	0.085	0.065	0.06	0.04	0.0337
Yield-to-Tensile Strength Ratio (f_y/f_u)	0.84	0.82	0.90	0.95	0.98	0.84

Table 2. Summary of measured values of local initial geometric defects in high-strength steel components

Author	Steel Grade	Flange Defect /B	Web Defect /H
Xu[14]	Q550	1/141	1/283
Han[15]	Q690	1/125	1/291
Xu[21]	Q800	1/153	1/263
Zhu[22]	Q460, Q550, Q690	1/238	1/420
Lin[23]	Q460, Q960	1/179	1/1085
Wang[24]	Q420, Q550, Q690, Q960	1/510	1/448
Zhou[25]	Q550	1/149	1/982
Average Value		1/213	1/539

Mesh division should consider both computational efficiency and accuracy; trials indicate that a 20mm mesh achieves satisfactory results. The input of welding residual stress affects the bending stiffness of steel components, and this section uses the uniform distribution model for welded I-

ISSN: 2414-1895 DOI: 10.6919/ICJE.202407_10(7).0010

shaped cross-section components of high-strength steel proposed by Ban[18]. Initial geometric imperfections in steel components are mainly caused by manufacturing errors and transportation. The "Code for Quality Acceptance of Steel Structure Engineering" GB 50205-2001 [20] sets clear permissible values for initial geometric imperfections in steel components. To more accurately simulate the actual conditions of the components, this study compiles local initial geometric imperfections of high-strength and ultra-high-strength steel components that meet the engineering construction quality acceptance standards, based on experiments by domestic and international scholars, as shown in Table 2. During finite element parameter analysis, the average values from Table 2 are used to introduce initial imperfections.

2.2 Finite Element Model Validation

The model validation was conducted through the four-point bending tests described by Xu [14] and Han [15]. The established models accounted for welding residual stresses and local initial geometric imperfections, incorporating necessary adjustments to align with the specific experimental setups. This process yielded key outcomes including the failure modes, moment-rotation curves, ultimate load capacities, and rotational capabilities of each component, which were then rigorously compared with the corresponding experimental results.

2.2.1 Failure Modes

Among the eleven components tested, the predominant failure mechanisms observed were local buckling and a combination of local buckling with global instability. Figs 4 and 5 showcase the failure mode comparisons for selected components. Notably, due to the wide spacing between lateral supports, the test specimen Y14 underwent local buckling and flexural-torsional buckling at mid-span. Similarly, specimens UM-460-1 and UM-460-2 exhibited local buckling failures at mid-span. The damage patterns simulated by the finite element models align well with these experimental observations, confirming the models' capability to accurately replicate the actual failure behaviors of the components.

(a) Overall comparison of failure modes (b) Local comparison of failure modes

Fig.4 Comparison of failure modes in test and FEA results of components Y14

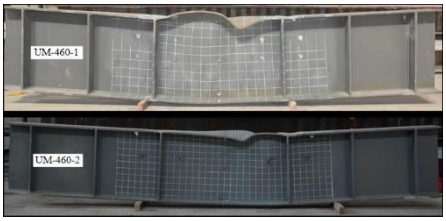

(a) Experimental failure modes

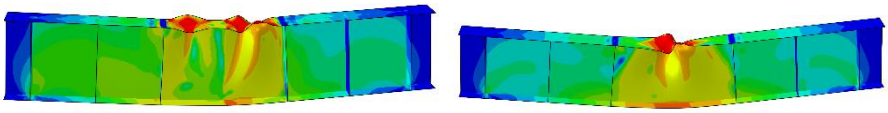

(b) Finite element model failure modes

Fig.5 Comparison of failure modes in test and FEA results of components UM-460-1, UM-460-2

ISSN: 2414-1895 DOI: 10.6919/ICJE.202407_10(7).0010

2.2.2 Moment-Rotation Curves

To verify if the finite element model can accurately simulate the mechanical response and deformation process of the test specimens, the computed moment-rotation curves from the finite element model were compared and analyzed against the experimental results. The moments and rotations were normalized against the full-section plastic moment (M_p) and plastic rotation (θ_p) of the components, yielding normalized moment-rotation curves for the components. Results for some components are displayed in Fig. 6. During the early loading phase, the normalized moment-rotation curves of the test components closely matched those simulated by the finite element model, confirming that the model's bending stiffness aligns well with that of the physical specimens. In the mid-loading phase, the differences in nominal bearing capacities were minimal. In the later stages of loading, the curves continued to decline due to local buckling. As friction from lateral supports adjacent to some test specimens increased with deformation, these components were more susceptible to the effects of friction in the later stages of loading, leading to slightly higher experimental normalized moment-rotation curves compared to those from the finite element simulation, although the differences were marginal.

Overall, the normalized moment-rotation curves obtained from the finite element calculations closely matched the experimental results, indicating that the modeling approach employed in this study can accurately simulate the mechanical response and deformation processes of bent members.

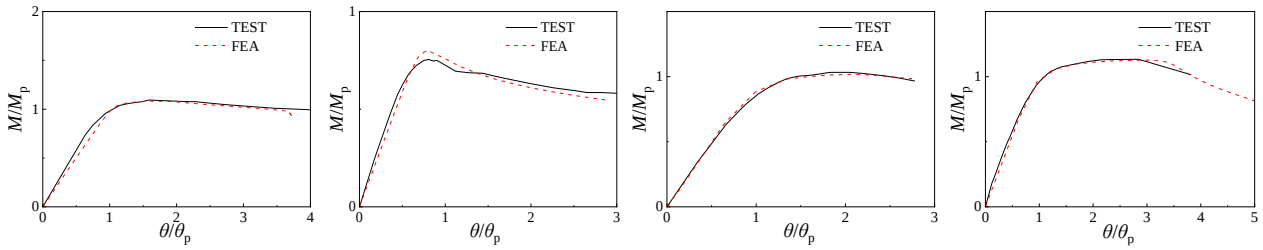

(a) UM-460-1 (b) UM-890-4 (c) Y11 (d) Y13

Fig.6 Comparison of moment-rotation curves in test and FEA results

2.2.3 Ultimate Bearing Capacity

The ultimate bearing capacity (M_u) and rotational capability (R) derived from finite element analysis were compared to experimental results as shown in Fig. 7, with specific data presented in Table 3. The calculation of rotational capacity employs the formula described in the subsequent section (Eq. 2). The average ratio of the finite element model's calculated ultimate bearing capacities to the experimental results reached 0.999. There was a slight discrepancy in the calculated rotational capabilities compared to the experimental results, primarily because the experimental specimens had lateral supports which increased their rotational capabilities; additionally, the initial imperfection modes applied in the model did not perfectly replicate the actual initial imperfections of the components, leading to some discrepancies. However, the overall average value was 1.013, suggesting that the modeling approach can adequately simulate the sectional performance of high-strength and ultra-high-strength steel components.

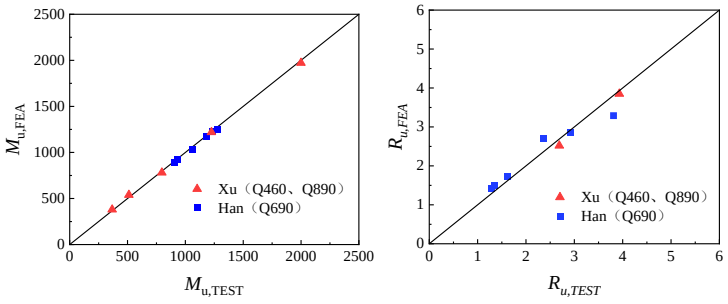

Fig.7 Comparison of test and FEA results

ISSN: 2414-1895 DOI: 10.6919/ICJE.202407_10(7).0010

Table 3. Comparison of test and FEA results

Author	Steel Grade	Component Number	$M_{u,TEST}$	$M_{u,FEA}$	$M_{u,FEA}/M_{u,TEST}$	$R_{u,TEST}$	$R_{u,FEA}$	$R_{u,FEA}/R_{u,TEST}$
Xu[14]	Q460	UM-460-1	1999.73	1972.36	0.986	2.69	2.52	0.937
		UM-460-2	1225.38	1219.88	0.996	3.93	3.85	0.980
	Q890	UM-890-4	797.10	781.18	0.980	--	--	--
		UM-890-5	511.90	539.23	1.053	--	--	--
		UM-890-6	367.31	379.89	1.034	--	--	--
Han[15]	Q690	Y11	903.60	889.68	0.985	1.28	1.42	1.109
		Y12	1065.00	1034.25	0.971	3.81	3.29	0.864
		Y13	1184.36	1175.99	0.993	2.36	2.70	1.144
		Y14	1274.10	1245.42	0.977	2.92	2.86	0.979
		Y15	928.30	928.38	1.000	1.61	1.73	1.075
		Y16	1232.50	1226.55	0.995	1.35	1.51	1.116
Average Value						0.999		1.013
Cov						0.021		0.092

Note: Mu, TEST is the ultimate bending moment of the component measured experimentally; Mu, FEA is the ultimate bending moment of the component obtained through finite element simulation.

In summary, the modeling approach adopted can effectively simulate the structural performance of the components.

2.3 Parameter Settings

To investigate the influence mechanisms of residual stress, local initial geometric imperfections, steel grade, and width-to-thickness ratio on the sectional performance of high-strength and ultra-high-strength steel bent members, primarily focusing on the effects on the section's ultimate bearing capacity (M_u) and rotational capacity (R), and to provide data support for subsequent section classification. Parameterized modeling is employed to accommodate various parameter settings, expanding the dataset to achieve more comprehensive and consistent results. The calculation of rotational capacity R refers to the formula (1) described in the following text.

Specific parameter settings were as follows: fixed section height H=400mm, B=200mm, flange width-to-thickness ratio $r_f=(b_f/t_f)$, web width-to-thickness ratio $r_w=(h_0/t_w)$, as illustrated in the sectional dimension diagram in Figure 8. A standard set of defect-free component simulation results served as the control group, with each steel grade having flange width-to-thickness ratios ranging from 3-12, and web width-to-thickness ratios from 20-120, comprising 180 component models in total. An equivalent number of models incorporated residual stresses and local initial geometric imperfections.

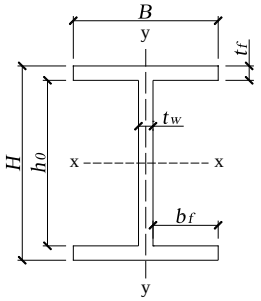

Fig.8 Definition of section dimensions

ISSN: 2414-1895 DOI: 10.6919/ICJE.202407_10(7).0010

For thorough parametric analysis to support subsequent sectional classification, the ranges for the flange width-to-thickness ratio and web width-to-thickness ratio were set from 3-13 and 10-120, respectively, to include new steel standards from S1-S5 sectional grades, with a total of 1512 models across various steel grades.

2.4 Parameter Analysis Results

Before classifying the sections, it is essential to analyze factors influencing the sectional performance of high-strength and ultra-high-strength steel bent members. This analysis provides a basis for considering these factors in subsequent finite element models and supports the accuracy of the upcoming sectional classification. This section examines and analyzes the impact mechanisms of welding residual stresses, local initial geometric imperfections, steel grades, and plate width-to-thickness ratios on sectional performance.

2.4.1 Welding Residual Stresses

Fig. 9 shows a comparison of the nominal ultimate bearing capacity (M_u/M_p) and rotational capabilities with and without welding residual stresses for Q800 steel components with a flange width-to-thickness ratio of 6. Welding residual stresses have a minimal impact on the sectional bearing capacity, with an average value of 0.992, but they significantly affect the rotational capabilities of the section. Table 4 presents average data from a comparative analysis of welding residual stress parameters across different steel grades, showing that the impact of welding residual stresses on sectional bearing capacity decreases with increasing steel grade.

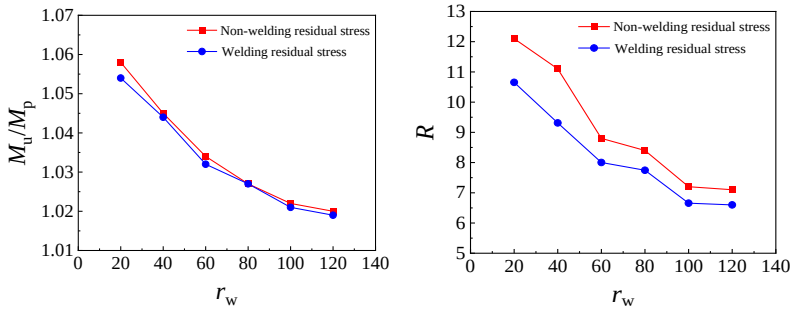

Fig.9 The influence of welding residual stress on the section performance of I-section bent members

Table 4. Comparison of residual stress parameter analysis results for different steel components

	$M_{u,RS}/M_u$					
	Q460	Q550	Q690	Q800	Q960	Q1100
Average Value	0.995	0.986	.0990	0.993	0.994	0.996
Overall average	0.992					

Note: Mu,RS, Mu are the ultimate bending moments of components with and without input of welding residual stresses, respectively.

2.4.2 Local Initial Geometric Imperfections

Fig. 10 illustrates the impact of local initial geometric imperfections on the nominal ultimate bearing capacity and rotational capabilities for Q800 steel at a flange width-to-thickness ratio of 6. Local imperfections significantly affect the nominal bearing capacity of the section, with an overall average of 0.901, and their influence on rotational capability increases as the web width-to-thickness ratio increases. Table 5 provides average data from a comparative analysis of local initial geometric imperfections across different steel grades, indicating that the impact of these imperfections on

ISSN: 2414-1895 DOI: 10.6919/ICJE.202407_10(7).0010

sectional bearing capacity grows with the steel grade, affecting higher strength steel sections more profoundly.

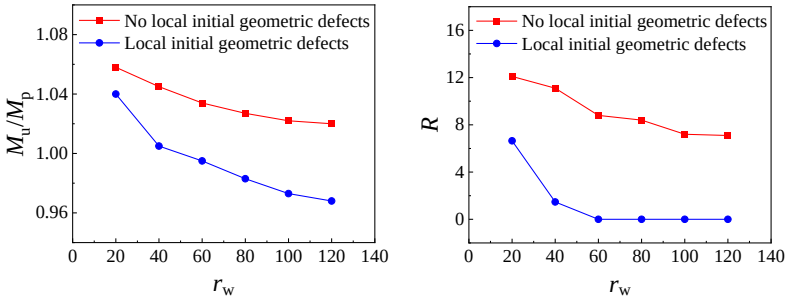

Fig.10 The influence of local initial geometric defects on the section performance of I-section bent members

Table 5. Comparison of parameter analysis results for local initial geometric imperfections in different steel components

	$M_{u,v}/M_u$					
	Q460	Q550	Q690	Q800	Q960	Q1100
Average	0.943	0.909	0.907	0.909	0.901	0.836
Overall average	0.901					

Note: Mu, v, Mu are the ultimate bending moments of components with and without local initial geometric defects, respectively.

2.4.3 Steel Grades

Fig. 11 depicts the influence of steel grades on the nominal ultimate bearing capacity for components at a flange width-to-thickness ratio of 6. As the steel grade increases, so does the yield strength and the yield-to-tensile strength ratio, while the ultimate strain decreases, thus diminishing the sectional plastic capability and decreasing both the nominal bearing capacity and the plastic deformation capacity. Due to the stress-strain model with a yield plateau used for Q460 steel, which has a slightly higher yield-to-tensile strength ratio compared to Q550 and Q1100, its plastic capability is relatively limited, resulting in a lower nominal ultimate bearing capacity. Conversely, Q1100 steel, with a lower yield-to-tensile strength ratio, exhibits higher plastic capabilities, leading to a higher nominal ultimate bearing capacity.

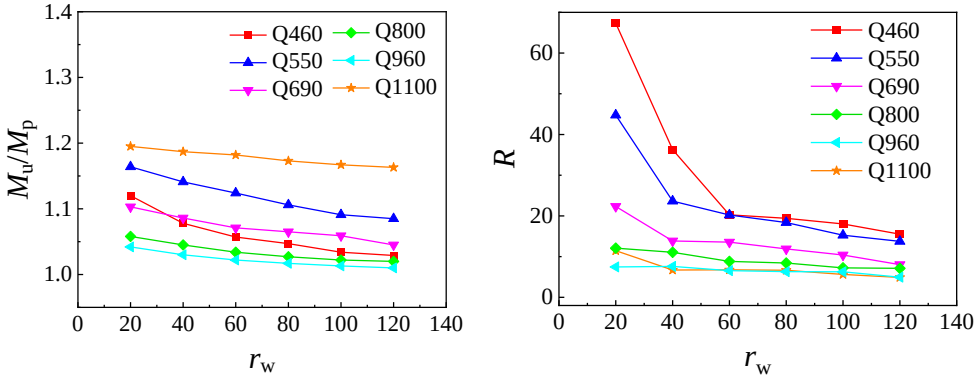

Fig.11 Impact of steel grades on the sectional performance of I-shaped bent members

ISSN: 2414-1895 DOI: 10.6919/ICJE.202407_10(7).0010

2.4.4 Plate Width-to-Thickness Ratio

The impact of flange and web aspect ratios on the cross-sectional performance of the component is depicted in Figs 12 and 13 respectively. It's clear that as the plate aspect ratio increases, the likelihood of local instability rises, resulting in a gradual reduction in both the nominal ultimate bearing capacity and rotational capacity of the component. Moreover, it's noticeable that with higher flange aspect ratios, coupled with increased web aspect ratios, the decline in nominal ultimate bearing capacity slows down. Similarly, as web aspect ratios rise alongside flange aspect ratios, the diminishing trend in nominal ultimate bearing capacity also decelerates. Overall, this underscores how the nominal ultimate bearing capacity of the specimens is intricately influenced by plate aspect ratios.

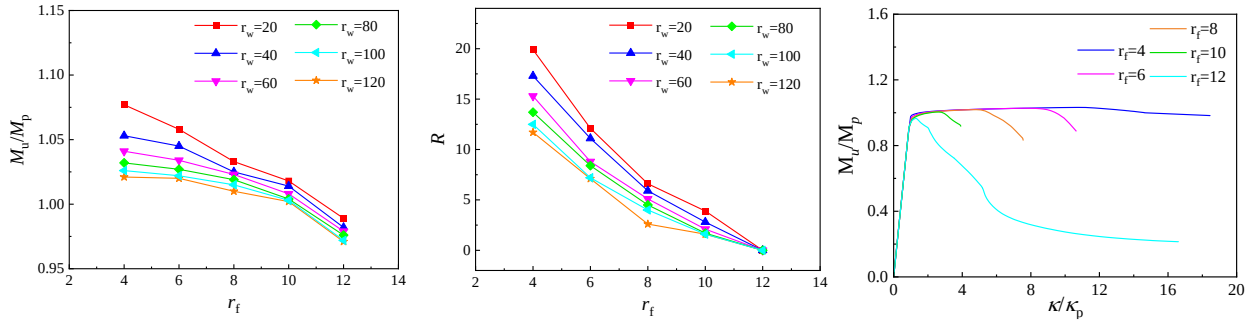

Fig.12 The influence of flange width-thickness ratio on the section performance of I-section bent members

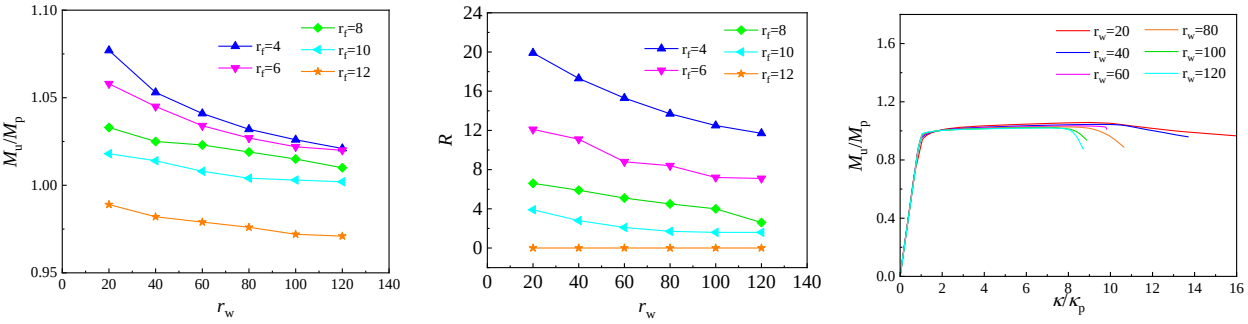

Fig.13 The influence of web width-thickness ratio on the section performance of I-section bent members

In conclusion, when calculating the sectional bearing capacity and plastic deformation rotational capability, the influences of welding residual stresses, local initial geometric imperfections, steel grades, and plate width-to-thickness ratios on sectional performance must be considered.

3. Section Classification Method and Width-to-Thickness Ratio Limits

Taking into account the relationships between panel components, as well as the influences of welding residual stresses and local initial geometric imperfections on sectional performance, the section classification is guided by the "Steel Structure Design Standard" GB50017-2017 [3]. Different section grades correspond to distinct performance requirements and are classified into five levels: S1, S2, S3, S4, and S5, as outlined in Table 6. Following the principle of uniform strength and in accordance with the "New Steel Standard"[3], width-to-thickness ratio limits for flanges and webs are adjusted when critical stresses reach yield stresses. The calculated width-to-thickness ratios for flanges and webs at critical buckling stresses are 18.46 and 137.61, respectively. These ratios, using the same adjustment coefficients as the "New Steel Standard"[3], form the basis for proposing section classifications suitable for high-strength and ultra-high-strength steel bent members.

ISSN: 2414-1895 DOI: 10.6919/ICJE.202407_10(7).0010

Table 6. Section classification and performance requirements

Section Grade	Sectional Performance	
S1	Full-Section plasticity achievable	Rotational capability reaches 7
S2	Full-Section plasticity achievable	-
S3	Entire flange yields, web can develop plasticity not exceeding 1/4 of the section height	-
S4	Edge fibers can reach yield strength, but plasticity cannot develop due to local buckling	-
S5	Web may undergo local buckling before edge fibers reach yield stress	-

For bent members, ductility is assessed at two levels: sectional ductility and component ductility, characterized using the section rotation capacity [26] and component rotation capacity [14] formulas, respectively. Internationally, section rotation capacity calculations are based on formula (1), and component rotation capacity calculations use formula (2).

$$R = \kappa_u/\kappa_p - 1 \tag{1}$$

$$R = \theta_u/\theta_p - 1 \tag{2}$$

In these formulas, κ_u is the curvature at which the moment-curvature curve descends to the full-section plastic moment M_p; κ_p is the curvature derived from dividing the full-section plastic moment M_p by the initial elastic stiffness, and θ_p is the corresponding angle at this point; θ_u is the angle when the component reaches the full-section plastic moment M_p. This study focuses on the sectional performance, specifically the sectional plastic deformation rotation capacity, thus formula (1) is employed for calculating section rotation capacity.

3.1 S1 Section Grade

The S1 section grade requires the section to reach the full-section plastic moment M_p, with a section rotation capacity R exceeding 7. The rotation capacities of numerous different steel grades, flange width-to-thickness ratios, and web width-to-thickness ratios are fitted into a surface model. Taking Q460 steel as an example, as shown in Fig. 14, the model fit R^2 is 0.94. The interaction between flange and web width-to-thickness ratios significantly affects sectional performance. Intersecting the surface with the target plane R=7 yields the S1 section grade boundary line (intersection curve L1). For practical engineering applications, this boundary line intersects with line $H1$=(137.61/18.46)r_f to determine the width-to-thickness ratio limits for various steel grades of S1 section grade.

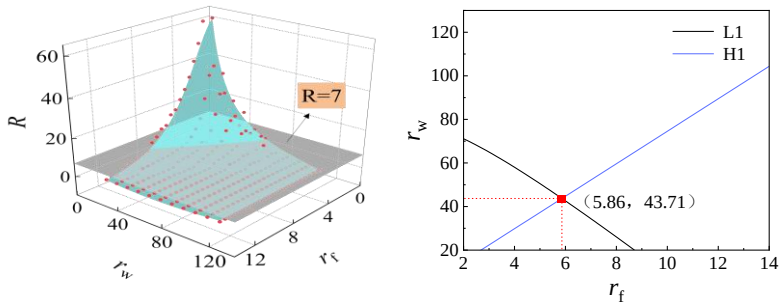

Fig.14 Width-to-thickness ratio limits for S1 section grade

ISSN: 2414-1895 DOI: 10.6919/ICJE.202407_10(7).0010

3.2 S2 Section Grade

The S2 section grade requires the section to reach the full-section plastic moment M_p without any specific requirements for section rotation capacity. Fitting the nominal bearing capacities M_u/M_p of various steel grades, flange width-to-thickness ratios, and web width-to-thickness ratios into a surface model, exemplified by Q460 steel in Fig. 15, achieves a model fit R^2 of 0.96. Intersecting this surface with the target plane $M_u/M_p=1$ yields the S2 section grade boundary line (intersection curve $L2$), which intersects with line $H1$ to determine the width-to-thickness ratio limits for various steel grades of S2 section grade.

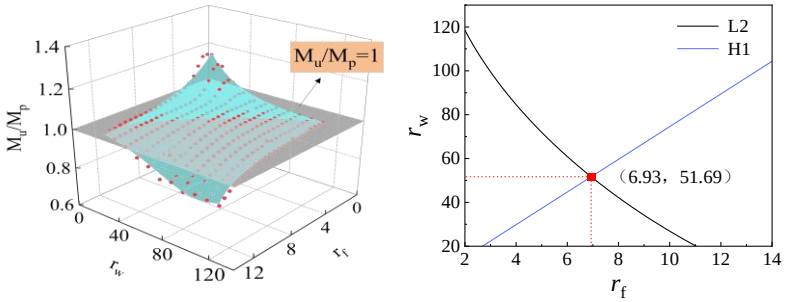

Fig.15 Width-to-thickness ratio limits for S2 section grade

3.3 S3 Section Grade

For the S3 section grade, the entire flange yields while the web develops plastic moment up to a quarter of the section height $M_{p,1/4}$. Fitting the nominal bearing capacities $M_{p,1/4}$ of different steel grades, flange width-to-thickness ratios, and web width-to-thickness ratios into a surface model, as shown for Q460 steel in Fig. 16, results in a model fit R^2 of 0.96. Intersecting this surface with the target plane $M_{p,1/4}=1$ yields the S3 section grade boundary line (intersection curve $L3$), which intersects with line $H1$ to determine the width-to-thickness ratio limits for various steel grades of S3 section grade.

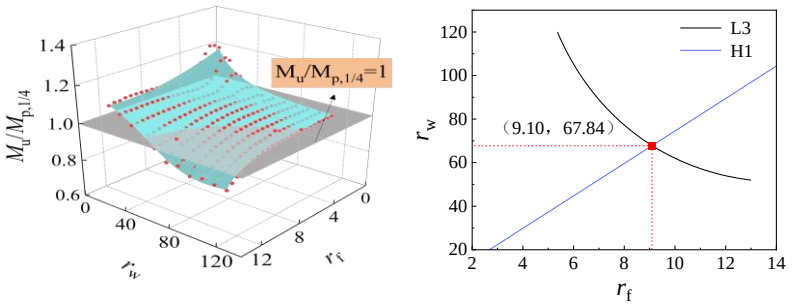

Fig.16 Width-to-thickness ratio limits for S3 section grade

3.4 S4 Section Grade

The S4 section grade requires the section edge fibers to reach yield strength, capable of achieving the elastic moment Me but unable to develop plasticity due to local buckling. Fitting the nominal bearing capacities M_u/M_e of different steel grades, flange width-to-thickness ratios, and web width-to-thickness ratios into a surface model, exemplified by Q460 steel in Fig. 17, achieves a model fit R^2 of 0.95. Intersecting this surface with the target plane $M_u/M_e=1$ yields the S4 section grade boundary line (intersection curve $L4$), which intersects with line $H1$ to determine the width-to-thickness ratio limits for various steel grades of S4 section grade.

ISSN: 2414-1895 DOI: 10.6919/ICJE.202407_10(7).0010

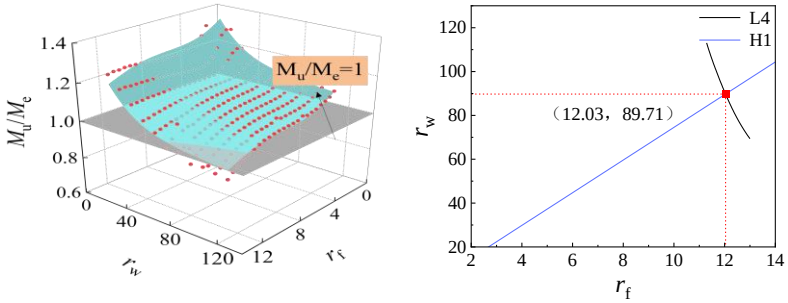

Fig.17 Width-to-thickness ratio limits for S4 section grade

3.5 Summary of Width-to-Thickness Ratio Limits

Table 7. Section classification and width-to-thickness ratio limits

Steel Grade	Steel Yield Strength(f_y/MPa)	r_f				r_w			
		S1	S2	S3	S4	S1	S2	S3	S4
Q460	460	5.9	6.9	9.1	12.0	43.7	51.7	67.8	89.7
Q550	550	5.6	7.1	8.8	10.5	42	52.8	65.5	78.2
Q690	690	5.0	6.73	7.9	9.6	37.6	50.2	59.2	71.8
Q800	800	4.3	6.3	7.4	9.0	32.3	47.2	55.0	66.8
Q960	960	3.5	6.0	6.9	8.1	26.0	44.6	51.7	60.2
Q1100	1100	3.6	6.4	6.9	7.7	26.5	47.5	51.1	57.4

Table 8. Recommendations for section classification and width-to-thickness ratio limits

Steel Grade	Flange					Web				
	S1	S2	S3	S4	S5	S1	S2	S3	S4	S5
Q460	$8\varepsilon_k$	$10\varepsilon_k$	$13\varepsilon_k$	$16\varepsilon_k$	20	$60\varepsilon_k$	$72\varepsilon_k$	$95\varepsilon_k$	$120\varepsilon_k$	250
Q550	$8\varepsilon_k$	$10\varepsilon_k$	$13\varepsilon_k$	$16\varepsilon_k$	20	$60\varepsilon_k$	$72\varepsilon_k$	$95\varepsilon_k$	$120\varepsilon_k$	250
Q690	$8\varepsilon_k$	$10\varepsilon_k$	$13\varepsilon_k$	$16\varepsilon_k$	20	$60\varepsilon_k$	$72\varepsilon_k$	$95\varepsilon_k$	$120\varepsilon_k$	250
Q800	$8\varepsilon_k$	$10\varepsilon_k$	$13\varepsilon_k$	$16\varepsilon_k$	20	$60\varepsilon_k$	$72\varepsilon_k$	$95\varepsilon_k$	$120\varepsilon_k$	250
Q960	$7\varepsilon_k$	$10\varepsilon_k$	$13\varepsilon_k$	$16\varepsilon_k$	20	$50\varepsilon_k$	$72\varepsilon_k$	$95\varepsilon_k$	$120\varepsilon_k$	250
Q1100	$7\varepsilon_k$	$13\varepsilon_k$	$14\varepsilon_k$	$16\varepsilon_k$	20	$50\varepsilon_k$	$100\varepsilon_k$	$110\varepsilon_k$	$120\varepsilon_k$	250

Note: εk is the steel grade correction coefficient., $\varepsilon_k = \sqrt{235/f_y}$.

The width-to-thickness ratio limits and classifications for bent members of various steel grades are summarized in Table 7. As the steel grade increases, reducing ductility and diminishing sectional plastic deformation capabilities, the width-to-thickness ratio limits become progressively stricter. Due to the presence of a yield plateau and a slightly higher yield-to-tensile strength ratio, Q460 steel has a more stringent width-to-thickness ratio limit for the S2 section grade. Q1100 steel, with a lower

ISSN: 2414-1895 DOI: 10.6919/ICJE.202407_10(7).0010

yield-to-tensile strength ratio and stronger post-yield plastic deformation capabilities, has higher width-to-thickness ratio limits for the S1 and S2 section grades compared to the Q960 grade.

For recommendations on width-to-thickness ratio limits for other steel grades, a steel grade correction coefficient $\varepsilon_k = \sqrt{235/f_y}$ is introduced. The normalized flange width-to-thickness ratio $\lambda_f = ((b_f/t_f)/\varepsilon_k)$ and the normalized web width-to-thickness ratio $\lambda_w = ((h_0/t_w)/\varepsilon_k)$ are set. For practical engineering applications, the I-shaped section bending component section grades and normalized width-to-thickness ratio limits incorporating the steel grade correction coefficient are unified and summarized in Table 8.

4. Section Classification Results Applicability Evaluation

The rationality and accuracy of the proposed section classification and width-to-thickness ratio limits for high-strength and ultra-high-strength steel components are assessed by comparing them with existing experimental results and both domestic and international standards.

4.1 Comparison with Existing Experimental Results

Based on the sectional performance requirements for each section grade defined in this study, experimental results from domestic and international researchers on the sectional performance of high-strength and ultra-high-strength steel bent members were classified and compared with the recommendations proposed in this article, as illustrated in Fig. 18. Fig. 18(a) compares the section classifications for Q800 and lower grade steels, while Fig. 18(b) does so for Q960 steel. The experimental data for Q960 steel are limited and require further expansion. Due to the lack of experimental data, in-depth research on Q1100 steel is needed.

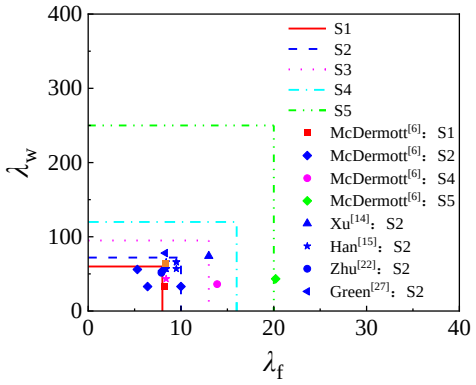

(a) Section classification comparison chart for steel grades up to Q800

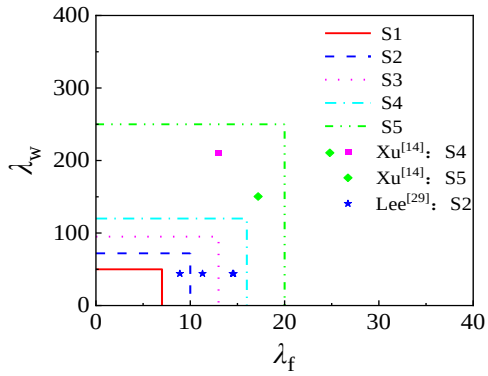

(b) Section classification comparison chart for Q960 Steel

Fig.18 Comparison of section classification limits with experimental data

ISSN: 2414-1895 DOI: 10.6919/ICJE.202407_10(7).0010

As demonstrated in the figures, the recommendations proposed in this article largely align with the experimental results, accurately achieving section classification and predicting sectional performance for high-strength and ultra-high-strength steel bent members.

4.2 Comparison with Standards

The "High Strength Steel Structure Design Standard" JGJT 483-2020 [4] is applicable for steels up to Q690, which requires the section classification of high-strength steel components to be designed according to the "Steel Structure Design Standard" GB50017-2017 [3]. The European Standard EC3 [28] covers steel grades up to S700 (with a standard yield strength of 700 MPa). Thus, the recommendations for width-to-thickness ratio limits for Q800 and lower steels proposed in this article are compared with these standards, as shown in Fig. 19.

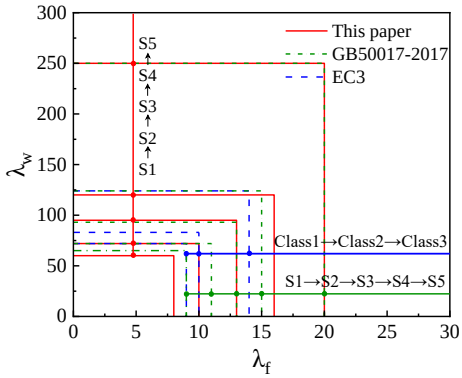

Fig.19 Comparison of section classification width-thickness ratio limits with international standards

The section classification and width-to-thickness ratio limits for Q800 and lower steels proposed in this article differ from those in GB50017-2017 [3]. Due to the high yield-to-tensile strength ratio, small plastic reserve, and reduced ultimate strain of high-strength and ultra-high-strength steels, their extent of plastic development and plastic deformation rotation capacity are lower. Therefore, the S1 and S2 section width-to-thickness ratio limits proposed in this article are stricter than those in the "New Steel Standard". Given that the recommendations consider the interaction between panels, the S4 section width-to-thickness ratio limits are relatively relaxed. Existing standards lack research on section classification for steels above Q690, and the rationality of the section classifications for these grades remains to be further investigated through experimental studies.

In summary, the section classification and width-to-thickness ratio limits proposed for high-strength and ultra-high-strength steel bent members in this article consider the material characteristics of these steels and the interaction between panels. The results are rational and facilitate engineering applications.

5. Conclusion

This study employed numerical simulation to develop a series of finite element models for I-shaped bent members made from high-strength and ultra-high-strength steels. It investigated the impact mechanisms influencing the sectional bearing capacity and plastic deformation rotational capability of these components, considering relevant factors, and proposed a section classification method and width-to-thickness ratio limits that account for panel interaction. The main conclusions are as follows:

The section classification suitable for high-strength and ultra-high-strength steels is based on the "Steel Structure Design Standard" GB50017-2017. Considering panel interactions, sections were divided into five grades: S1, S2, S3, S4, S5, with corresponding width-to-thickness ratio limits proposed.

ISSN: 2414-1895 DOI: 10.6919/ICJE.202407_10(7).0010

Due to the high yield-to-tensile strength ratio and small ultimate strain of high-strength and ultra-high-strength steels, their plastic development is limited and plastic deformation rotational capability is reduced. The width-to-thickness ratio limits for S1 and S2 section grades proposed for Q800 and lower steels are stricter compared to GB50017-2017 [3]. Since the interaction between flange and web panels was considered, the S4 section grade width-to-thickness ratio limits are more relaxed.

The section classification and width-to-thickness ratio limits proposed for high-strength and ultra-high-strength steel I-shaped bent members can effectively predict sectional bearing capacity and plastic deformation rotational capability, providing references for the seismic performance-oriented design of these materials.

References

[1] LI G Q. Progress of research on high-strength structural steel connections[J].Steel Construction(Chinese & English), 2020, 35(6): 1-40.

[2] CHENG X, HOU X S, LI Z F. Cross-section classification criteria of steel H-sections considering the plate interaction effect[J]. Engineering Mechanics, 2020, 37(4): 178-185.

[3] Standard for design of steel structures: GB50017-2017[S]. Beijing: China Architecture & Building Press, 2017. (in Chinese).

[4] Standard for design of high strength steel structures: JGJ/T483-2020[S]. Beijing: China Architecture & Building Press, 2020. (in Chinese).

[5] Mcdermott J F. Local plastic buckling of A514 steel members[J]. Journal of the Structural Division, Proceedings of the American Society of Civil Engineers, 1969, 95(9): 1837-1850.

[6] McDermott J F. Plastic bending of A514 steel beams[J]. Journal of the Structural Division, Proceedings of the American Society of Civil Engineers, 1969, 95(9).

[7] Beg D, Hladnik L. Slenderness limit of Class 3 I cross-sections made of high strength steel[J]. Journal of Constructional Steel Research, 1996, 38(3): 201-217.

[8] Ricles J M, Sause R, Green P S. High-strength steel: implications of material and geometric characteristics on inelastic flexural behavior [J]. Engineering Structures, 1998, 20(4): 323-335.

[9] Earls C J. On the inelastic failure of high strength steel I-shaped beams[J]. Journal of Constructional Steel Research, 1999, 49(1): 1-24.

[10] Thomas S J, Earls C J. Cross-sectional compactness and bracing requirements for HPS483Wgirders[J]. Journal of Structural Engineering, 2003, 129(12): 1569-1583.

[11] Shokouhian M, Shi Y. Classification of I-section flexural members based on member ductility[J]. Journal of Constructional Steel Research, 2014, 95: 198-210.

[12] TONG G S, FU B. Ductility factors of plates and section classification for seismic design[J]. Engineering Mechanics, 2013, 30(03): 323-330.

[13] Xiong G, Feng Y, Peng Q, et al. Lateral-torsional buckling behaviour of 690 MPa high strength steel beams[C]//Structures. Elsevier, 2021, 33: 3999-4010.

[14] XU K L. Local buckling behaviour and design method of high strength steel welded I-section beams[D]. Beijing: Tsinghua University, 2017.

[15] HAN Q. Investigation on bending resistance and ductility of Q690 high strength steel welded H-section beam[D]. Chongqing: School of Civil Engineering of Chongqing University, 2019.

[16] HOU X S, Cross-sections classification criteria of steel H-sections considering plate interaction effect and multi-directional loading[D]. Taiyuan: Taiyuan University of Technology, 2020.

[17] SHI G, ZHU X. Study on constitutive model of high-strength structural steel under monotonic loading[J]. Engineering Mechanics, 2017, 34(2): 50-59.

[18] YIN F. Mechanical properties and design method of welded I-section members of ultra high strength steel with 1100MPa yield strength[D]. Beijing: Beijing University of Technology, 2023.

[19] BAN H Y, SHI G, SHI Y J. Experimental and unified model investigations on residual stress within high strength steel welded I-sections[J]. Engineering Mechanics, 2014, 31(8): 83-91.

ISSN: 2414-1895 DOI: 10.6919/ICJE.202407_10(7).0010

[20] Code for quality acceptance of steel structure engineering construction. GB50205-2001[S]. Beijing: China Architecture & Building Press, 2001. (in Chinese).

[21] XU Y. Research on the buckling behavior of 800MPa High-strength Steel Welded I-section Members under Axial Compression[D]. Anhui: Anhui University of Technology, 2018.

[22] ZHU H. Research on flexural bending capacity and ductility of hybrid-steel I-shaped beams of Q690 high-strength steel[D]. Chongqing: Chongqing University, 2022.

[23] LIN C C. Local buckling and design method of high strength steel weld-section members under axial compression[D]. Beijing: Tsinghua University, 2012.

[24] WANG J. Buckling behaviour of welded H-section and box section members with high-strength steel under axial compression[D]. Chongqing: Chongqing University, 2022.

[25] ZHOU C. Research on local and local-overall buckling behavior of Q550 weld I-section members under axial Compression[D]. Nanjing: Southeast University, 2016.

[26] Gardner L, Theofanous M. Discrete and continuous treatment of local buckling in stainless steel elements[J]. Journal of Constructional Steel Research, 2008, 64(11): 1207-1216.

[27] Green P S. The inelastic behavior of flexural members fabricated from high performance steel [Doctoral thesis]. Bethlehem: Lehigh University, 2000.

[28] British Standards Institution. BS EN 1993-1-1. Eurocode 3: Design of steel structures: Part 1-1: General rules and rules for buildings. London: BSI, 2005.

[29] Lee G C, Galambos T V. Post-buckling strength of wide-flange beams. Journal of the Engineering Mechanics Division, 1962, 88(1): 59-75.